

# Universal properties of quasi-one-dimensional excitons in semiconducting single-walled carbon nanotubes and $\pi$ -conjugated polymers

H. Zhao<sup>1</sup>, S. Mazumdar<sup>1</sup>, C.-X. Sheng<sup>2</sup>, and Z. V. Vardeny<sup>2</sup>

<sup>1</sup>Department of Physics, University of Arizona, Tucson, AZ 85721

<sup>2</sup>Department of Physics, University of Utah, Salt Lake City, UT 84112

Corresponding author: Sumit Mazumdar

Department of Physics, University of Arizona, Tucson, AZ 85721

Telephone: (520) 621-6803, Fax: (520) 621-4721, Email: [sumit@physics.arizona.edu](mailto:sumit@physics.arizona.edu)

## Abstract

The nature of the primary photoexcitations in semiconducting single-walled carbon nanotubes (S-SW CNTs) is of strong current interest. We have studied the emission spectra of S-SW CNTs and two different  $\pi$ -conjugated polymers in solutions and films, and have also performed ultrafast pump-probe spectroscopy on these systems. The emission spectra relative to the absorption bands are very similar in S-SW CNTs and polymers, with red-shifted photoluminescence in films showing exciton migration. The transient photoinduced absorptions (PA s) in SW CNTs and  $\pi$ -conjugated polymers are also remarkably similar, with a low energy PA<sub>1</sub> and a higher energy PA<sub>2</sub> in all cases. Theoretical calculations of excited state absorptions within a correlated  $\pi$ -electron Hamiltonian find the same excitonic energy spectrum for S-SW CNTs and  $\pi$ -conjugated polymers, illustrating the universal features of quasi-one-dimensional excitons in carbon-based  $\pi$ -conjugated systems. In both cases PA<sub>1</sub> is an excited state absorption from the optically allowed exciton to a two-photon exciton that occurs below the continuum band threshold. PA<sub>1</sub> therefore gives the lower limit of the binding energy of the lowest optical exciton. The binding energy of lowest exciton belonging to the widest S-SW CNTs with diameters  $\geq 1$  nm in films is 0.3{0.4 eV, as determined by both experimental and theoretical methods.

# 1 Introduction

Single-walled carbon nanotubes (SW CNTs) are of considerable current interest because of their unique mechanical [1], electrical [2] and optoelectronic [3, 4] properties. Metallic versus semiconducting character of SW CNTs are determined by their chiralities, but in all cases extended dimensions along the tube axes and nanometer scale diameters render these systems quasi-one-dimensional (quasi-1D). Spatial separation of SW CNTs has recently become possible [5], and this has led to intensive studies of the photophysics of the semiconducting SW CNTs (S-SW CNTs). Different experiments have begun to indicate that the primary photoexcitations in these systems are excitons, and not the free electrons and holes that are expected within one-electron theory [6]. Exciton formation in S-SW CNTs is a direct consequence of the combined effects of Coulomb electron-electron (e-e) interaction and the confinement that occurs in 1D. It is, for example, well known that confinement effects in 1D lead to unconditional exciton formation upon electron-hole (e-h) excitation, and excitons in nanowires of conventional semiconductors have been described within the 1D hydrogenic model, with deep exciton states and discrete energy spectrum below a Rydberg continuum [7]. Recent theories of linear optical absorptions in S-SW CNTs have emphasized the strong e-h interactions and the consequent exciton formation in these systems [8, 9, 10, 11, 12, 13, 14].

In spite of the above theoretical and experimental investigations, the knowledge base about the physical nature of the optical excitons or the complete excitonic energy spectrum in S-SW CNTs remains incomplete. Whether or not the 1D hydrogenic model can be applied without modifications to S-SW CNTs is unclear, and there is also no consensus as yet on important materials parameters such as the exciton binding energy. One important reason for this is that the standard technique of comparing the thresholds of linear absorption and photoconductivity for the determination of the exciton binding energy fails in noncrystalline organic materials because of the existence of disorder and inhomogeneity in these systems. More recent experimental probes of S-SW CNTs have therefore focused on nonlinear absorption, which can give information on the nature of excited states occurring above the optical exciton. Several research groups have performed transient photomodulation (PM) experiments [15, 16, 17, 18, 19], which have provided valuable information on the excitation dependence of photoluminescence (PL) and radiative versus nonradiative relaxation channels. A two-photon fluorescence measurement has given the first information on the lowest two-photon state that occurs above the lowest optical exciton in S-SW CNTs with diameters within a certain range [20]. Experimental results here were interpreted within the context of the 1D hydrogenic model. Joint experiment-theory work on electroabsorption in S-SW CNTs

has recently been performed [21].

It is relevant in this context to recall that there exists already a vast literature on excitons in the  $\pi$ -conjugated polymers, the other class of carbon-based quasi-1D systems. In order to seek guidance from this knowledge base, we have performed precisely the same transient PM experiments with S-SW CNTs that were previously performed with the polymers [22, 23]. We have also performed theoretical calculations of the excited state electronic structures and excited state absorptions for ten different S-SW CNTs with a wide range in diameters, within the same correlated electron model that has been widely applied to  $\pi$ -conjugated polymers [24, 25, 26, 27, 28, 29, 30, 31]. We find a one-to-one correspondence in the excitonic energy spectra of S-SW CNTs and  $\pi$ -conjugated polymers, in spite of the fact that the carbon nanotubes are derived from 2D graphitic layers and the coordination number per carbon atom is 3 instead of 2.

In the following sections we present the results of our experimental and theoretical investigations. We begin by pointing out the similarities in the linear optical absorption and fluorescence in S-SW CNTs and two different  $\pi$ -conjugated polymers. Following this, we present the results of our ultrafast pump-probe measurements on the same systems. Remarkable similarities between the S-SW CNTs and  $\pi$ -conjugated polymers are found. Finally, we present our theoretical work within the context of a correlated  $\pi$ -electron Hamiltonian. We briefly review the known results for the excitonic energy spectrum of  $\pi$ -conjugated polymers within the model Hamiltonian, and then proceed to discuss our new results obtained for the S-SW CNTs. Our main message is that there exists a universality in the photophysics of these two classes of systems with quasi-1D excitons. Our results and conclusions also suggest possible directions for future optical investigations of S-SW CNTs.

## 2 Experimental setup

### 2.1 Sample preparation

In order to measure the ultrafast dynamic response of unbundled SW CNTs in the mid-IR spectral range (0.1 to 1.0 eV), it was necessary to fabricate a transparent solid sample in the broadest spectrum possible that contains isolated nanotubes. To achieve this, 0.005% HiPCO-produced SW CNTs were mixed with 0.610% SDS surfactant and 0.865% poly-vinyl alcohol (PVA) in de-ionized water. Sonication for an hour before sample preparation resulted in relatively well-separated nanotubes as evident by the sharp features in the absorption spectrum (Fig. 1b). We then deposited a film of the solution onto CaF<sub>2</sub> by drop-casting

at 80 °C. The film consisted of well-separated SWCNTs embedded in an insulating matrix of PVA having an optical density of 1 in the visible/near-IR spectral range (Fig. 1). Neither PVA nor SDS has absorption bands in the spectral range over which we measured the absorption and transient PL spectra. Resonant Raman scattering of the radial breathing mode was used to determine that the nanotubes in our sample have a diameter distribution around a mean diameter of 0.8 nm, and contain about 1/3 metallic and 2/3 semiconducting SWCNTs.

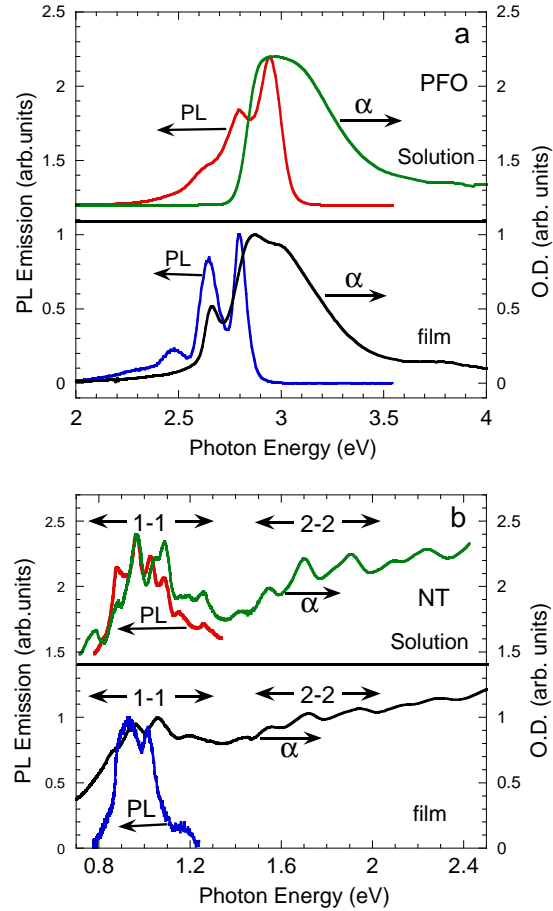


Figure 1: Photoluminescence (PL) emission and absorption (O.D.) spectra of (a) PFO solution and film, and (b) isolated SWCNTs in  $D_2O$  solution and PVA matrix film. The optical transitions 1-1 and 2-2 for SWCNT are assigned.

Dispersions of predominantly isolated nanotubes in  $D_2O$  were prepared using a procedure based on the method developed by O'Connell et al. [5]. The sonicated samples were first centrifuged for 10 min at 700 g. The upper 75% of the supernatant was recovered using a small-bore pipette, avoiding sediment at the bottom, and transferred to a Beckman centrifuge

tube for further centrifugation. Samples were then centrifuged for 2 hr at 4 °C. The upper 50% of the supernatant was then recovered using a small-bore pipette, avoiding sediment at the bottom, and transferred to a clean tube.

The semiconducting polymers used in our studies were a poly(phenylene-vinylene) (PPV) derivative, viz., dioctyloxy-PPV (DOO-PPV) that was synthesized in our laboratory using a published procedure [32], and a blue poly(9,9-dioctyl fluorene) (PFO) derivative that was purchased from American Dye Corp. (Canada) and used as is. Solutions were obtained by dissolving the polymer powder in toluene with concentration of 1 mg/ml; films were obtained from the solution drop-casting onto CaF<sub>2</sub> substrates.

## 2.2 The optical setup

For our transient PM measurements we used the fs two-color pump-probe correlation technique with linearly polarized light beams from two different experimental setups based on Ti:sapphire lasers, with a broad spectral range from 0.1 to 2.6 eV and 100 fs time resolution that was not possible before. To achieve such a broad spectral range we used two laser systems: a low power high repetition rate laser with energy per pulse of about 0.1 nJ that was used for the mid-IR spectral range; and a high power low repetition rate laser with energy/pulse of about 10 J that was used in the near-IR to visible spectral range. The transient PM spectra from the two laser systems were normalized to each other at several probe wavelengths in the near-IR spectral range. The ultrafast laser system used for the low power measurements was a 100 fs Ti:sapphire oscillator (Tsunami, Spectra-Physics) operating at a repetition rate of about 80 MHz, which pumped an optical parametric oscillator (Opal, Spectra-Physics). The Opal generates signal (S) and idler (I) beams that were used as probes with photon energy  $\hbar\omega_S$  and  $\hbar\omega_I$  ranging between 0.55 and 1.05 eV. In addition, these two beams were also mixed in a nonlinear crystal (AgGaS<sub>2</sub>) to generate probe at  $\omega_{\text{probe}} = \omega_S - \omega_I$  in the spectral range of 0.13 to 0.43 eV. The pump beam for SWCNT was the fundamental at 1.6 eV; whereas for the polymers we used the second harmonic of the fundamental at 3.2 eV. The low energy/pulse produces low photoexcitation density of the order of  $10^{16} \text{ cm}^{-3}$ . With such low density we avoided the problem of exciton-exciton annihilation that could complicate the decay dynamics, or two-photon absorption (TPA) processes that may generate photoexcitations with very large excess energy. To increase the signal/noise ratio, an acousto-optical modulator operating at 85 kHz was used to modulate the pump beam intensity. For measuring the transient response at time  $t$  with 150 fs time resolution, the probe pulses were mechanically delayed with respect to the pump pulses

using a translation stage; the time  $t = 0$  was obtained by a cross-correlation between the pump and probe pulses in a nonlinear optical crystal. The transient PM signal,  $T = T(t)$  is the fractional change in transmission,  $T$ , which is negative for photoinduced absorption (PA) and positive for photoinduced bleaching (PB) and stimulated emission (SE). The pump and probe beams were carefully adjusted to get complete spatial overlap on the film, which was kept under dynamic vacuum. In addition, the pump/probe beam-walk with the translation stage was carefully monitored and the transient response was adjusted by the beam walk measured response.

For the visible and near-IR measurements we used a home-made Ti:sapphire laser amplifier system that operates at 1 kHz. The laser beam was split into two beams. The main part of the laser beam (96%) was used as is for pumping the SWCNT samples, or frequency doubled in a non-linear crystal to 3.2 eV for pumping the polymer samples. The other 4% of the amplifier output generated white light super-continuum pulses in a glass substrate within the spectral range from 1.2 to 2.6 eV that was used as a probe. The pump and probe beams were carefully adjusted to get complete spatial overlap on the sample.

For measuring the PL spectra we used a standard cw setup comprised of a pump laser (Ar<sup>+</sup> laser for the polymers and Ti:sapphire for the SWCNT sample), a  $\frac{1}{4}$ -meter monochromator and solid-state detectors (Si diode for the polymers and Ge diode for the SWCNT). A phase sensitive technique was used to enhance the signal/noise ratio. The absorption spectra were measured with commercially available spectrometers.

## 3 Experimental Results

### 3.1 Linear absorption and fluorescence

We begin our comparison of the optical properties of  $\pi$ -conjugated polymers and S-SWCNTs with a discussion of the absorption ( $\epsilon$ ) and PL spectra of PFO and SWCNTs, in solutions and films (see Fig. 1). In all cases the spectra are inhomogeneously broadened. The lowest optical gap of S-SWCNTs is in the mid-IR spectral range, whereas that of PFO is in the blue region of the visible spectral range. Within the one-electron tight-binding model [6] the 1-1 optical absorption band in SWCNTs is due to dipole allowed transitions from the highest valence subband to the lowest conduction subband, whereas the 2-2 transitions are from the next highest valence subband to the next lowest conduction subband, respectively. It is well known that the absorption bands of M-SWCNTs appear at  $h\nu > 1.6$  eV, and thus the S-SWCNTs in our films are preferentially excited by the pump pulses at  $h\nu = 1.6$  eV.

In contrast to the SW CNT films, (!) of SW CNTs in D<sub>2</sub>O solution (Fig. 1b) contains a number of distinct sub-bands. This shows that the inhomogeneity of the SW CNTs in D<sub>2</sub>O solution is smaller than that in the film. It is likely that in the solution the nanotubes are bunched together in specific groups with similar diameters, and thus exhibit more structured (!) than in the film.

In agreement with Kasha's rule [33], which states that light emission occurs from the lowest energy level that is dipole-coupled to the ground state, PL emission bands in both PFO and SW CNT samples appear close to the low end of the (!). In the PFO solution spectra (Fig. 1a) the PL 1-1 band that occurs on the high energy side of the spectrum actually overlaps with the absorption band. The PFO film contains two phases of different polymer order ( and ), where shows PL at lower energies [34]. The PL bands of both phases are redshifted relative to their respective absorption bands. As in the PFO solution, in the SW CNT solution spectrum (Fig. 1b) also the PL bands overlap with their respective 1-1 absorption bands. In the SW CNT film, in contrast, the PL bands are again redshifted with respect to their corresponding absorption bands, exactly as in the PFO film. The underlying mechanism of the redshifted PL band in PFO films was identified as exciton migration to the lowest energy sites [35]. Based on the redshifted PL emission in the SW CNT film, we therefore speculate that here too there occur excitons that migrate to the lowest energy \emission sites." The ease of exciton migration in both materials shows that the excitons are robust, with binding energies substantially larger than the binding energies of the shallow traps in the sample.

### 3.2 Ultrafast spectroscopy measurements

In Fig. 2 we compare the transient PM spectra of films of S-SW CNTs and two polymers at time  $t = 0$ . The PM spectra contain both negative (PA) and positive (PB or SE) bands. In neither sample do we obtain a PA spectrum that increases at low energy in the shape of free carrier absorption, viz.,  $\propto \lambda^{-2}$ . Instead, the PA spectra are in the form of distinct photoinduced bands PA<sub>1</sub> and PA<sub>2</sub> associated with specific optical transitions of the primary photoexcitations in the samples, which are therefore not free carriers. The sharp PA rise below 0.2 eV is likely due to photogenerated \free" carrier absorption in M-SW CNTs. The free carriers may have been separated in the M-SW CNTs following the original exciton photogeneration in the S-SW CNTs, and their consequent diffusion among various SW CNTs in the sample.

The PA and their respective PB (or SE) bands in both polymers and S-SW CNTs are



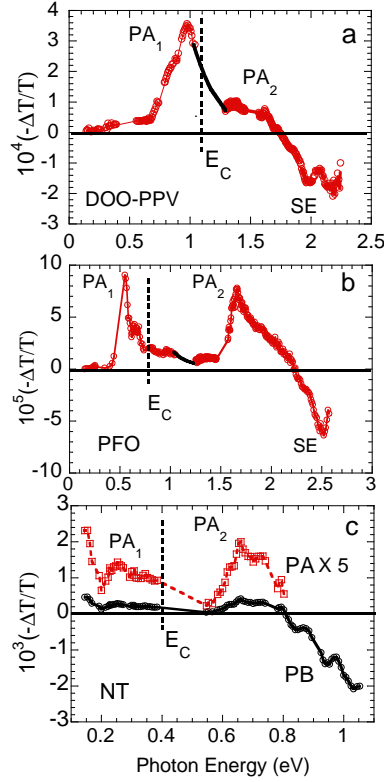


Figure 2: Transient PM spectra at  $t = 0$  of  $\ln s$  of DOO-PPV (a), PFO (b), and isolated SW CNT in PVA matrix (c). Various PA, PB, and SE bands are assigned. The vertical dashed lines at  $E_C$  between  $PA_1$  and  $PA_2$  denote the estimated continuum band onset (see text).

correlated to each other (see Fig. 3). The lack of SE in the S-SW CNT PM spectrum shows that whereas excitons in polymers are radiative, excitons in the S-SW CNTs are not. The dominance of nonradiative over radiative recombination in S-SW CNT has been ascribed to a variety of effects including, (a) trapping of the excitation at defect sites [6], (b) strong electron-phonon coupling [37], and (c) the occurrence of optically dark excitons below the allowed excitons [13]. Furthermore, from the correlated dynamics of the transient PB and PA bands we have previously concluded that PA originates from excitons in the  $n = 1$  manifold [16, 18].

Fig. 3 summarizes the decay dynamics of the various bands in the PM spectra of these semiconductors. For each material the PA, PB or SE bands have very similar dynamics and therefore they share a common origin, namely, the same primary excitation, which is the photogenerated exciton. In the case of polymer  $\ln s$  (Fig. 3 a and b)  $PA_1$ ,  $PA_2$  and SE decays are non-exponential, with the decay in DOO-PPV longer than that in PFO. It has

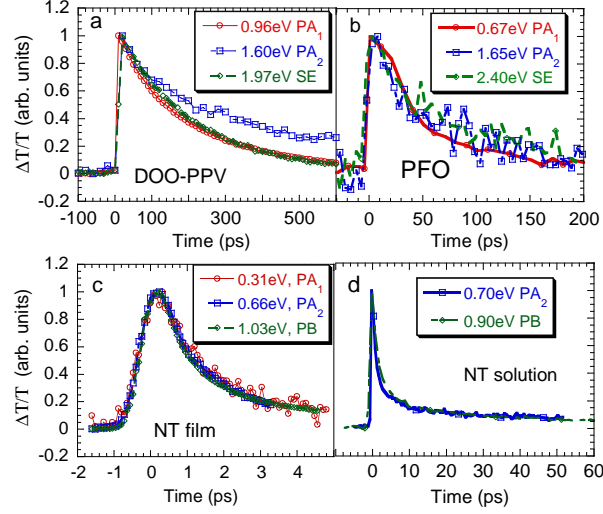


Figure 3: Transient PM dynamics at various probe energies in (a) DOO-PPV, (b) PFO, (c) SW CNT in PVA matrix, and (d) SW CNTs in  $D_2O$  solution.

been empirically determined that the decay time constant in the  $\pi$ -conjugated polymers is related to the PL quantum efficiency (QE) by the relation [38]:

$$\tau_{\text{PM}} = \tau_{\text{rad}} / \text{QE}; \quad [1]$$

where  $\tau_{\text{rad}}$  ( $\sim 1,000$  ps) is the radiative lifetime of the 1D exciton [22, 23]. We estimate  $\tau_{\text{PPV}} = 250$  ps (Fig. 3a),  $\tau_{\text{PFO}} = 100$  ps (Fig. 3b), and get  $\text{QE} = 25\%$  in DOO-PPV and  $\text{QE} = 10\%$  in PFO; both  $\tau$ 's are in excellent agreement with the PL QE that we measured using an integrated sphere.

Figs. 3 c and d show the decay dynamics of the photogenerated exciton in S-SW CNT film and solution, respectively. The decay in the S-SW CNT film is much faster ( $\sim 2$  ps), and this is probably caused by exciton migration in SW CNT bundles from S-SW CNTs to M-SW CNTs, the energy relaxation rate in which is relatively fast and non-radiative. The exciton decay in S-SW CNTs in solution (Fig. 3d) is composed of a fast and slow component, similar to the recently measured PL(t) decay [39]. The correlation of transient PM and PL again shows that the PA is due to excitons in this material. We determined that the slow component PA lasts ca. 0.5 ns. From Eq. 1 for the QE of 1D excitons in  $\pi$ -conjugated polymers and  $\tau_{\text{rad}} = 1,000$  ps we calculate  $\text{QE} = 50\%$  for S-SW CNTs. The PL QE in S-SW CNTs in solution was, however, measured to be  $6 \times 10^{-4}$ , and this indicates that the radiative lifetime  $\tau_{\text{rad}}$  for excitons in S-SW CNTs is very different than that in polymers.

Actually from the measured  $\tau_{\text{rad}} \approx 1$  ps, and the slow PA component lifetime we calculate using Eq. 1, indicating that the bulk of the  $n = 1$  excitons that contribute to PA are nonradiative. This seems to support the previous suggestion that rapid decay occurs in S-SW CNTs from the optical to the dark exciton with lower energy [13].

## 4 $\pi$ -electron exciton theory and photophysics

### 4.1 Theoretical model

The striking similarities in the transient PM spectra and cw PL with respect to  $(\lambda)$  spectra of the polymeric semiconductors and the SW CNTs strongly suggest that the two families of materials should be described within the same fundamental theory. Common to both SW CNTs and semiconducting polymers are  $\pi$ -electrons, and we anticipate that the optical behavior is determined predominantly by these electrons. While  $\pi$ -electron-only models miss the curvature effects associated with the narrowest SW CNTs, the low peak energy of the  $\text{PA}_1$  band in Fig. 2c indicates that the photophysics of the S-SW CNTs in our sample is dominated by the widest SW CNTs (see below). We will thus be interested in generic consequences of e-e interactions that are valid for the widest S-SW CNTs. We therefore focus on the semiempirical Pariser-Parr-Pople (PPP) model Hamiltonian [40, 41], which has been widely applied to  $\pi$ -conjugated systems in the past,

$$H = \sum_{hij} t_{ij} (c_i^\dagger c_j + c_j^\dagger c_i) + U \sum_i n_i n_{i\#} + \frac{1}{2} \sum_{i \neq j} V_{ij} (n_i - 1)(n_j - 1): \quad [2]$$

Here  $c_i^\dagger$  ( $c_i$ ) creates (annihilates) a  $\pi$ -electron on carbon atom  $i$  with spin  $(\uparrow, \downarrow)$ ,  $hij$  implies nearest neighbor (n.n.) sites  $i$  and  $j$ ,  $n_i = c_i^\dagger c_i$  is the number of electrons with spin  $\uparrow$  on site  $i$ , and  $n_i = \sum_{\uparrow\downarrow} n_i$  is the total number of electrons on site  $i$ . The parameter  $t_{ij}$  is the hopping integral between  $p_z$  orbitals of n.n. carbon atoms,  $U$  is the on-site Coulomb repulsion between two electrons occupying the same carbon atom  $p_z$  orbital, and  $V_{ij}$  is the long-range intersite Coulomb interaction. In the case of the  $\pi$ -conjugated polymers  $t_{ij}$  are different for phenyl, single and double carbon bonds. For the SW CNTs, however they are the same. Longer range  $t_{ij}$  beyond n.n. can be included in Eq. 2, but previous experience indicates that these terms have only quantitative effects and do not give additional insight.

The main advantage of using the semiempirical  $\pi$ -electron model over ab initio approaches is that exciton effects and excited state absorptions can be calculated directly within the

sem empirical Hamiltonian. The photophysics and nonlinear absorptions of  $\pi$ -conjugated polymers have been widely investigated within Eq. 2 [24, 25, 26, 27, 28, 29, 30, 31], and very recently a theory of linear absorption in S-SW CNTs was advanced within this model [13]. It is useful to first briefly discuss the theory of linear and nonlinear absorptions in  $\pi$ -conjugated polymers within the PPP model.

## 4.2 Excitons and excited state energy spectra of $\pi$ -conjugated polymers

Unsubstituted  $\pi$ -conjugated polymers usually possess inversion symmetry and eigenstates are thus classified as even parity  $A_g$  and odd parity  $B_u$ . Fig. 4a shows schematically the theoretical excitation spectra of a light emissive  $\pi$ -conjugated polymer such as PFO or PPV [29]. Optical transitions corresponding to  $PA_1$  and  $PA_2$  are indicated as vertical arrows in the figure. The spin singlet ground state is  $1^1A_g$ . The lowest optical state  $1^1B_u$  is an exciton. Although eigenstates within Eq. 2 are correlated, the  $1^1B_u$  is predominantly a one electron-one hole (1e-1h) excitation relative to the correlated ground state [42]. The lowest two-photon state, the  $2^1A_g$ , is highly correlated and has strong contributions from triplet-triplet two electron-two hole (2e-2h) excitations [42]. There can occur other low energy 2e-2h triplet-triplet two-photon states above the  $2^1A_g$ , but all such two-photon states participate weakly in PA or TPA, because of their weak dipole-couplings to the 1e-1h  $1^1B_u$ . A different higher energy two-photon state (see Fig. 4a), referred to as the  $m^1A_g$  (where  $m$  is an unknown quantum number), has an unusually large dipole coupling with the  $1^1B_u$  and has been shown theoretically to dominate nonlinear absorption measurements [24, 25, 26, 31, 42]. The  $m^1A_g$  is the lowest predominantly 1e-1h two-photon exciton, and is characterized by greater e-h separation than in the  $1^1B_u$  [42]. The lower threshold state of the continuum band in Fig. 4a is referred to as the  $n^1B_u$  [25, 42]. Although there exist many other excited states in the infinite polymer, theory predicts that the  $1^1A_g$ ,  $1^1B_u$ ,  $m^1A_g$  and  $n^1B_u$  are the four essential states [24, 25, 26, 27, 28, 29, 30, 31] that dominate the optical nonlinearity because of the very large dipole couplings among them.

Based on direct computations [29],  $PA_1$  in PPV and PFO corresponds to excited state absorption from the  $1^1B_u$  optical exciton to the  $m^1A_g$  two-photon exciton within the correlated electron picture. The  $m^1A_g$  exciton has been experimentally observed in PA [22, 23], TPA [43], electro-absorption [25, 44]. Notice that Fig. 4a indicates that  $PA_1$  gives the lower limit of the exciton binding energy. Given the widths of the experimental  $PA_1$  bands in Fig. 2 a and b, and the theoretical uncertainty in the energy difference between the contin-

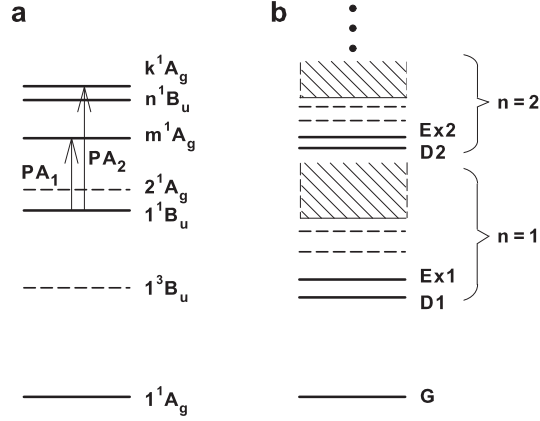


Figure 4: Schematics of the excitonic electronic structures of (a) a light-emissive  $\pi$ -conjugated polymer and (b) a S-SW CNT. In (a) the lowest triplet exciton  $1^3B_u$  occurs below the lowest singlet exciton  $1^1B_u$ . The lowest two-photon state  $2^1A_g$  is composed of two triplets and plays a weak role in nonlinear absorption. Transient PA is from the  $1^1B_u$  to the  $m^1A_g$  two-photon exciton which occurs below the continuum band threshold state  $n^1B_u$ , and to a high energy  $k^1A_g$  state that occurs deep inside the continuum band. In (b),  $Ex_n$  and  $D_n$  are dipole-allowed and forbidden excitons, respectively.

uum band threshold and the  $m^1A_g$ , we believe that the exciton binding energy is  $0.8 \pm 0.2$  eV in PPV-DOO and  $0.6 \pm 0.2$  eV in PFO.

$PA_2$  in  $\pi$ -conjugated polymers is to a distinct  $k^1A_g$  state that occurs deep inside the continuum band. Theoretical description of this state has been given by Shukla et al. [45]. Specifically, in polymers with multiple bands within one-electron theory, there occur multiple classes of 2e-2h excited configurations, involving different bands. The exact  $m^1A_g$  and  $k^1A_g$  are both superpositions of 1e-1h and 2e-2h excitations, but the natures of the 2e-2h excitations that contribute to these states are different.

The results shown schematically in Fig. 4a have been obtained by solving the Hamiltonian of Eq. 2 using a variety of sophisticated many-body techniques. Based on comparisons of exact and approximate finite chain wavefunctions, we have shown that eigenstates that are predominantly 1e-1h relative to the correlated ground state can be described semiquantitatively within the single configuration-interaction (SCI) approximation [27, 29], which retains only the configuration mixing between 1e-1h excitations from the Hartree-Fock (H-F) ground state. We have used the SCI approximation to understand the essential states in S-SW CNTs, which, as mentioned above, are 1e-1h.

### 4.3 Linear absorption and one-photon excitons in S-SW CNTs

We have recently calculated the linear absorptions of different S-SW CNTs with diameters ( $d$ ) ranging from 0.55 to 1.35 nm within the PPP model of Eq. 2, using the SCI approximation [13]. The list includes seven zigzag semiconductors between the (7,0) and the (17,0) SW CNTs (inclusive), and the (6,2), (6,4) and (7,6) chiral SW CNTs. Our calculations were for the standard value of  $t_{ij} = t = 2.4$  eV. Our parametrization of the  $V_{ij}$  was similar to the standard Ohno parametrization [46]

$$V_{ij} = -\frac{U}{1 + 0.6117R_{ij}^2}; \quad [3]$$

where  $R_{ij}$  is the distance between sites  $i$  and  $j$  in  $A$ , and  $\epsilon$  is a measure of the dielectric screening due to the medium [29]. Based on our fitting of linear, nonlinear and triplet absorptions in PPV [29], we chose  $U = 8.0$  eV and  $\epsilon = 2$  in our S-SW CNT calculations [13].

In Fig. 4b we show schematically a summary of our calculations. There occur multiple energy manifolds  $n = 1, 2, \dots$  etc., within the total energy scheme. Within each  $n$ , there occur optically dark excitons  $D_n$  a few  $k_B T$  below the optically allowed exciton  $E_n$ . Each manifold  $n$  has also its own H-F band gap that corresponds to the lower threshold of the continuum band within SCI theory. The binding energies of the excitons are then defined as the energy difference between the H-F band gaps and the excitons within the same manifold. We found that the binding energies of the  $n = 1$  and  $n = 2$  excitons decrease with increasing diameters, and they are nearly equal in the wide S-SW CNT limit. Our calculated binding energies for S-SW CNTs were in all cases smaller than those calculated for PPV or PFO using the same parameters. For the widest S-SW CNTs ( $d = 1.3$  nm), our calculated exciton binding energies are close to 0.3 eV.

### 4.4 Nonlinear absorption in S-SW CNTs

In the present work we performed SCI calculations of excited state absorptions using the parameters of Eq. 3, for all the S-SW CNTs in reference [13]. The zigzag S-SW CNT calculations are for 18-20 unit cells, whereas the chiral S-SW CNT calculations are for 10 unit cells. We have confirmed that convergence in energies has been reached at these sizes. Zigzag S-SW CNTs possess inversion symmetry, and therefore eigenstates are once again classified as  $A_g$  and  $B_u$ . Lack of inversion symmetry in chiral S-SW CNTs implies that their eigenstates are not strictly one- or two-photon states. Nevertheless, we have found from explicit

calculations that even in the chiral S-SW CNTs eigenstates are predominantly one-photon (with negligible two-photon cross-section) and predominantly two-photon (with very weak one-photon dipole coupling to the ground state). We shall therefore refer to chiral S-SW CNT eigenstates as  $A_g$  and  $B_u$ , respectively.

The nature of the ultrafast PA discussed in the previous section demonstrates that PA is due to excited state absorption from the  $n = 1$  exciton states. From Fig. 4b, the excited state absorption can be from  $Ex1$ , as well as from  $D1$ , following rapid nonradiative decay of  $Ex1$  to  $D1$ . As in the case of  $\pi$ -conjugated polymers [42], we have evaluated all transition dipole couplings between the  $n = 1$  exciton states ( $Ex1$  and  $D1$ ) and all higher energy excitations. The overall results for S-SW CNTs are very similar to those in the  $\pi$ -conjugated polymers.

Our computational results are the same for all zigzag nanotubes. These are modified somewhat for the chiral nanotubes (see below), but the behavior of all chiral S-SW CNTs are again similar. In Figs. 5a and b we show the representative results for the zigzag (10,0) and the chiral (6,2) S-SW CNTs, respectively. The solid vertical lines in Fig. 5a indicate the magnitudes of the normalized dipole couplings between  $Ex1$  in the (10,0) NT with all higher energy excitations  $e_j$ ,  $\langle Ex1 | j \rangle \langle j | i \rangle = \langle Ex1 | j \rangle \langle j | G \rangle$ , where  $G$  is the ground state. The dotted vertical lines are the normalized transition dipole moments between the dark exciton  $D1$  and the higher excited states,  $\langle D1 | j \rangle \langle j | i \rangle = \langle D1 | j \rangle \langle j | G \rangle$ . Both couplings are shown against the quantum numbers  $j$  of the final state along the lower horizontal axis, while the energies of the states  $j$  are indicated on the upper horizontal axis. The reason why only two vertical lines appear in Fig. 5a is that all other normalized dipole couplings are invisible on the scale of the figure. A striking aspect of the results for the (10,0) zigzag S-SW CNT are then that exactly as in the  $\pi$ -conjugated polymers, the optical exciton  $Ex1$  is strongly dipole-coupled to a single higher energy  $m^1A_g$  state. The dark exciton  $D1$  is similarly strongly coupled to a single higher energy state (hereafter the  $m^0A_g$ ). Furthermore, the dipole couplings between  $Ex1$  and  $m^1A_g$  (or  $D1$  and  $m^0A_g$ ) are stronger than those between the ground state and the excitons, which is also true for the  $\pi$ -conjugated polymers [42].

The situation in the chiral (6,2) S-SW CNT is slightly different, as shown in Fig. 5b. Both the  $Ex1$  and  $D1$  excitons are now strongly dipole-coupled to several close-lying excited states, which form narrow "bands" of  $m^1A_g$  and  $m^0A_g$  states. Similar to the case of zigzag S-SW CNTs, these bands occur above the  $Ex1$ .

From the calculated results of Fig. 5 a simple interpretation to  $PA_1$  in Fig. 2 emerges, viz.,  $PA_1$  is a superposition of excited state absorptions from  $Ex1$  and  $D1$ . This raises the question whether  $PA_2$  in the S-SW CNTs can be higher energy inter-subband absorptions

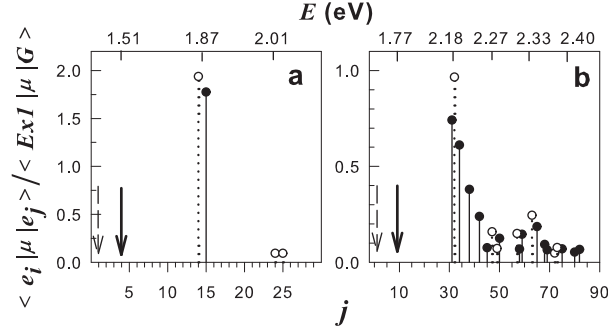


Figure 5: Normalized transition dipole moments between S-SW CNT exciton states  $Ex1$  and  $D1$  and all other excited states  $e_j$ , where  $j$  is the quantum number of the state in the total space of single excitations from the H-F ground state. The numbers along the upper horizontal axes are energies in eV. Results shown are for (a) the (10,0), and (b) the (6,2) S-SW CNTs, respectively. Solid (dotted) lines correspond to  $e_i = Ex1$  ( $D1$ ). The solid and dashed arrows denote the quantum numbers of  $Ex1$  and  $D1$ , respectively.

from the  $n = 1$  excitons to two-photon states that lie in the  $n = 2$  (or even  $n = 3$ ) manifolds. We have eliminated this possibility from explicit calculations: the transition dipole matrix elements between one-photon states in the  $n = 1$  manifold and two-photon states within the higher  $n$  manifolds are zero. As in the  $\pi$ -conjugated polymers, two-photon states giving rise to  $PA_2$  cannot therefore be computationally accessed without taking into account the  $2e-2h$  excitations [45] and are outside the scope of the present work.

In Fig. 6 we show the energy locations of all the relevant one- and two-photon states within the  $n = 1$  manifold for the (10,0) and (6,2) NTs. The figure includes the absolute energies of the  $Exn$  and  $Dn$  excitons, the two-photon  $m^1A_g$  states and the corresponding H-F bandgaps for the (10,0) and (6,2) S-SW CNTs. We did not include in Fig. 6 the  $m^0A_g$  states that are coupled to the dark excitons, as they will be indistinguishable in their energies from the  $m^1A_g$  states on this scale. For comparison, we have also included in the figure the excitonic energy spectrum of PPV, calculated within the PPP Hamiltonian of Eq. 2 with the same parameters. Within SCI theory, all states below the H-F thresholds within the same manifold are excitons. For the (10,0) zigzag S-SW CNT we have also shown the higher energy  $n^1B_u$  state in the  $n = 1$  manifold. As with the  $\pi$ -conjugated polymers, this state is identified by its large dipole couplings with the  $m^1A_g$ . Importantly, in both the (10,0) and the (6,2) S-SW CNTs, the  $m^1A_g$  and  $m^1A_g''$  states occur below the respective H-F thresholds, indicating that exactly as in the  $\pi$ -conjugated polymers, the energy locations of these excitonic two-photon states give the lower bound to the exciton binding energy.

In Table 1 we have summarized the calculated results for all the S-SW CNTs we have



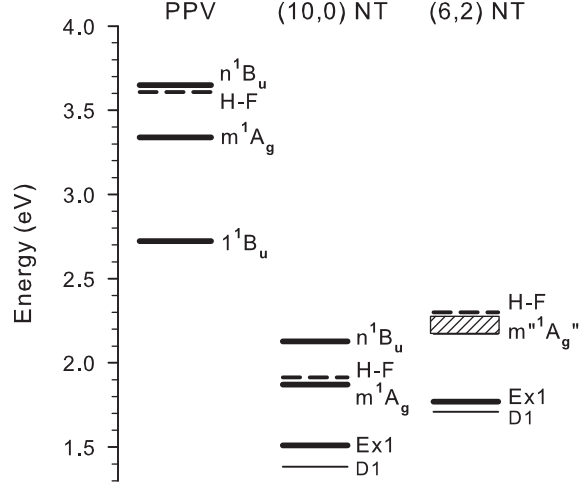


Figure 6: SC I energies of optically relevant states in (from left to right) PPV, (10,0) SW CNT and (6,2) SW CNT, respectively. In all cases the  $m^1A_g$  ( $m^1A_g''$ ) is an exciton and  $PA_1$  gives the lower limit of the exciton binding energy.

studied. We give the calculated PA energies that originate from both the Ex1 and the D1 excitons, as well as the corresponding H-F thresholds for the  $n = 1$  manifold. Note that for S-SW CNTs with diameters 0.8–1.3 nm, the calculated range of PA energies, 0.25–0.55 eV, matches closely with the experimental width of the  $PA_1$  band in Fig. 2. As we have already indicated,  $PA_2$  is not due to excited state absorption from the  $n = 1$  excitons to states in the higher manifold, and this indicates that the most likely origin of  $PA_2$  is the same as that in PPV. In Fig. 2 we have indicated that the continuum band threshold in PPV and PFO lies in between  $PA_1$  and  $PA_2$ , in view of both theoretical and experimental work. Based on the overall experimental similarities that we find between the  $\pi$ -conjugated polymers and S-SW CNTs, and the theoretical energy spectra, it is then natural to guess that the location of the  $n = 1$  continuum band threshold in S-SW CNTs also lies between the peaks of the  $PA_1$  and  $PA_2$  absorption bands. This would give lowest exciton binding energies of about 0.3 eV in the widest S-SW CNTs, in excellent agreement with the calculations.

## 5 Discussions and conclusions

Our principal conclusion is that the energy spectrum within the  $n = 1$  energy manifold of S-SW CNTs is very similar to the energy spectrum of  $\pi$ -conjugated polymers. The origin of the low energy  $PA_1$  in both S-SW CNTs and  $\pi$ -conjugated polymers is then excited state absorption from EX1 and D1 to higher energy two-photon excitons. The broad nature of

NT	d (Å)	$E_{PA_1}^{Ex1}$ (eV)	$E_{PA_1}^{D1}$ (eV)	$E_{bl}$ (eV)
(7,0)	5.56	0.42	0.54	0.54
(6,2)	5.72	0.41	0.44	0.53
(8,0)	6.35	0.37	0.47	0.53
(6,4)	6.92	0.36	0.41	0.48
(10,0)	7.94	0.36	0.49	0.41
(11,0)	8.73	0.31	0.40	0.41
(7,6)	8.95	0.28	0.33	0.39
(13,0)	10.3	0.31	0.43	0.32
(14,0)	11.1	0.28	0.37	0.34
(17,0)	13.5	0.27	0.35	0.29

Table 1: Summary of computed results for different SW CNTs. Here  $E_{PA_1}^{Ex1}$  and  $E_{PA_1}^{D1}$  are  $PA_1$  energies that correspond to excited state absorptions from the Ex1 and D1, respectively.  $E_{bl}$  is the binding energy of Ex1, as measured by the energy difference between the H-F band threshold and the energy of Ex1.

the  $PA_1$  band in the S-SW CNTs arises from the inhomogeneous nature of the experimental sample, with SW CNT bundles that contain a distribution of S-SW CNTs with different diameters and exciton binding energies. If we assume that the peak in the  $PA_1$  band corresponds to those S-SW CNTs that dominate nonlinear absorption, then the low energy of the peak in the  $PA_1$  band in Fig. 2, taken together with the data in Table 1, suggest that  $PA_1$  is dominated by the widest S-SW CNTs in our sample. The common origin of  $PA_1$  and  $PA_2$  (see Fig. 3) indicates that  $PA_2$  is also dominated by the widest S-SW CNTs. The peak in the  $PA_2$  band at  $\sim 0.7$  eV then is due to the widest S-SW CNTs, with  $PA_2$  due to narrower S-SW CNTs occurring at even higher energies. Hence the energy region  $0.2\{0.55$  eV in Fig. 2c must correspond only to  $PA_1$  excitations. Based on the similarities in the energy spectra of the S-SW CNTs and the  $\pi$ -conjugated polymers in Fig. 6, we can therefore construct the vertical dashed line in Fig. 2c, which identifies the threshold of the continuum band for the widest S-SW CNTs in the film. Exciton binding energies of ca. 0.4 eV are then predicted for those S-SW CNTs in the film that dominate the nonlinear absorption. For S-SW CNTs with diameters  $\sim 0.8$  nm, Wang et al. found TPA at energies very close to the peak of our  $PA_1$  band, and based on additional estimates from the 1D hydrogenic exciton theory, determined their exciton binding energies to be also ca. 0.4 eV [20]. Remarkably, our calculated binding energies of the excitons for S-SW CNTs with diameters in this range are very close in Table 1. We believe that this coincidence in the calculated and observed experimental exciton binding energies for the S-SW CNTs is not fortuitous. Within the PPP Hamiltonian the

exciton binding energy depends primarily on the long range Coulomb interactions in Eq. 3. The parametrization of Eq. 3 for PPV was arrived at following an extensive search across fifteen sets of  $(U; \epsilon)$  values in reference [29], and only the parameter set  $U = 8.0$  eV,  $\epsilon = 2.0$  reproduced all four linear absorption bands (at 2.4, 3.7, 4.7 and 6.0 eV, respectively) and the experimentally observed energies of the  $m^1A_g$  [22, 23] and the  $1^3B_u$  [47]. The successful transferability of the parameters from PPV to S-SW CNTs then suggests that the Coulomb interaction parameters as well as the background dielectric constants in these two classes of materials are close in magnitude. This in turn justifies the use of  $\pi$ -electron models for the S-SW CNTs, at least for the widest S-SW CNTs which dominate the nonlinear absorption.

The similarity in the photophysics of S-SW CNTs and  $\pi$ -conjugated polymers suggests several directions for future research. Theoretically, determination of the proper mechanism of  $PA_2$  in analogy to the existing results for  $\pi$ -conjugated polymers [45] is a high priority. The energy location of the lowest triplet exciton and triplet  $PA$  energy in S-SW CNTs are also of strong experimental and theoretical interest. The energy difference between the lowest singlet and triplet excitons is a measure of the strength of Coulomb interactions, while calculations of triplet  $PA$  provide yet another check for the model Hamiltonian of Eq. 2. S-SW CNTs also provide us with a unique opportunity of extending nonlinear spectroscopy to the very interesting region of the  $n = 2$  energy manifolds. Exciton states in the  $n = 2$  manifold lie deep inside the  $n = 1$  continuum band and can be expected to exhibit novel optical behavior. Whether or not the  $n = 2$  manifold has the same structure as the  $n = 1$  manifold is an intriguing question. Although neither TPA nor PM experiments can reach the two-photon states in this region, these should become visible in electro-absorption measurements. Theoretical and experimental works along these directions are currently in progress.

## 6 Acknowledgments

We thank Ray H. Baughman and Alan B. Dalton (Nanotech Institute, UT Dallas) for supplying the SW CNT samples, and M. Tong for help with the ps measurements in the visible spectral range. Work at the University of Arizona was supported by NSF-DMR-0406604. Work at the University of Utah was supported by DOE-FG-04-ER46109.

## References

1. Dalton, A. B., Collins, S., Muñoz, E., Razal, J. M., Ebron, V. H., Ferraris, J. P., Coleman, J. N., Kinn, B. G., & Baughman, R. H. (2003) *Nature* 423, 703.
2. Collins, P. G., Zettl, A., Bando, H., Thess, A., & Smalley, R. E. (1997) *Science* 278, 100{103.
3. Mieswich, J. A., Martel, R., Avouris, Ph., Tsang, J. C., Heinze, S., & Terso, J. (2003) *Science* 300, 783{786.
4. Hertel, T. & Moos, G. (2000) *Phys. Rev. Lett.* 84, 5002{5005.
5. O'Connell, M. J., Bachilo, S. M., Human, C. B., Moore, V. C., Strano, M. S., Haroz, E. H., Riabin, K. L., Boul, P. J., Noon, W. H., Kittrell, C., et al. (2002) *Science* 297, 593{596.
6. Saito, R., Dresselhaus, G., & Dresselhaus, M. S. (1998) *Physical Properties of Carbon Nanotubes* (Imperial College Press, London).
7. Ogawa, T. & Takagahara, T. (1991) *Phys. Rev. B* 44, 8138{8156.
8. Ando, T. (1997) *J. Phys. Soc. Jpn.* 66, 1066{1073.
9. Lin, M. F. (2000) *Phys. Rev. B* 62, 13153{13159.
10. Kane, C. L. & Mele, E. J. (2003) *Phys. Rev. Lett.* 90, 207401.
11. Spataru, C. D., Ismail-Beigi, S., Benedict, L. X., & Louie, S. G. (2004) *Phys. Rev. Lett.* 92, 077402.
12. Chang, E., Bussi, G., Ruini, A., & Molinari, E. (2004) *Phys. Rev. Lett.* 92, 196401.
13. Zhao, H. & Mazumdar, S. (2004) *Phys. Rev. Lett.* 93, 157402.
14. Perebeinos, V., Terso, J., & Avouris, Ph. (2004) *Phys. Rev. Lett.* 92, 257402.
15. Lauret, J.-S., Voisin, C., Cassabois, G., Delalande, C., Roussignol, P., Jost, O., & Capes, L. (2003) *Phys. Rev. Lett.* 90, 057404.
16. Korovyanko, O. J., Sheng, C.-X., Vardeny, Z. V., Dalton, A. B., & Baughman, R. H. (2004) *Phys. Rev. Lett.* 92, 017403.
17. Ma, Y.-Z., Stenger, J., Zimmermann, J., Bachilo, S. M., Smalley, R. E., Weisman, R. B., & Fleming, G. R. (2004) *J. Chem. Phys.* 120, 3368{3373.
18. Sheng, C.-X., Vardeny, Z. V., Dalton, A. B., & Baughman, R. H. (2005) *Phys. Rev. B* 71, 125427.

19. Manzoni, C., Gambetta, A., Menna, E., Meneghetti, M., Lanzani, G., & Cerullo, G. (2005) Phys. Rev. Lett. 94, 207401.
20. Wang, F., Dukovic, G., Brus, L.E., & Heinz, T.F. (2005) Science 308, 838{841.
21. Kennedy, J.W., Vardeny, Z.V., Collins, S., Baughman, R.H., Zhao, H., & Mazumdar, S. (2005) cond-mat/0505071.
22. Frolov, S.V., Bao, Z., Wohlgenannt, M., & Vardeny, Z.V. (2000) Phys. Rev. Lett. 85, 2196{2199.
23. Frolov, S.V., Kloc, C., Batlogg, B., Wohlgenannt, M., Jiang, X., & Vardeny, Z.V. (2001) Phys. Rev. B 63, 205203.
24. Dixit, S.N., Guo, D., & Mazumdar, S. (1991) Phys. Rev. B 43, 6781{6784.
25. Guo, D., Mazumdar, S., Dixit, S.N., Kajzar, F., Jarka, F., Kawabe, Y., & Peyghambarian, N. (1993) Phys. Rev. B 48, 1433{1459.
26. McWilliam, P.C.M., Hayden, G.W., & Soos, Z.G. (1991) Phys. Rev. B 43, 9777{9791.
27. Abe, S., Schreiber, M., Su, W.P., & Yu, J. (1992) Phys. Rev. B 45, 9432{9435.
28. Beljonne, D., Comil, J., Shuai, Z., Bredas, J.L., Rohl ng, F., Bradley, D.D.C., Torruellas, W.E., Ricci, V., & Stegeman, G.I. (1997) Phys. Rev. B 55, 1505{1516.
29. Chandross, M., Mazumdar, S., Liess, M., Lane, P.A., Vardeny, Z.V., Hamaguchi, M., & Yoshino, K. (1997) Phys. Rev. B 55, 1486{1496; Chandross, M. & Mazumdar, S. (1997) Phys. Rev. B 55, 1497{1504.
30. Ramasesha, S., Pati, S.K., Shuai, Z., & Bredas, J.L. (2000) Adv. Quantum Chem. 38, 121{215.
31. Race, A., Barford, W., & Bursill, R.J. (2001) Phys. Rev. B 64, 035208.
32. Hamaguchi, M. & Yoshino, K. (1994) Jpn. J. Appl. Phys. 33, L1478{L1481.
33. Kasha, M. (1950) Discuss. Faraday Soc. 9, 14{19.
34. Cadby, A.J., Lane, P.A., Melbr, H., Martin, S.J., Grell, M., Giebeler, C., Bradley, D.D.C., Wohlgenannt, M., An, C., & Vardeny, Z.V. (2000) Phys. Rev. B 62, 15604{15609.
35. Hidayat, R., Tatsuhashi, S., Kim, D.W., Ozaki, M., Yoshino, K., Teraguchi, M., & Masuda, T. (2000) Phys. Rev. B 61, 10167{10173.
36. Wang, F., Dukovic, G., Brus, L.E., & Heinz, T.F. (2004) Phys. Rev. Lett. 92, 177401.
37. Htoon, H., O'Connell, M.J., Doom, S.K., & Klimov, V.I. (2005) Phys. Rev. Lett. 94, 127403.

38. Pankove, J. I. (1971) Optical Processes in Semiconductors (Prentice-Hall, Englewood Cliffs, N.J.).
39. Reich, S., Dworzak, M., Homann, A., Thom sen, C., & Strano, M .S. (2005) Phys. Rev. B 71, 033402.
40. Pariser, R. & Parr, R. G . (1953) J. Chem . Phys. 21, 466{471.
41. Pople, J. A . (1953) Trans. Faraday Soc. 49, 1375{1385.
42. Chandross, M., Shim oi, Y., & Mazum dar, S. (1999) Phys. Rev. B 59, 4822{4838.
43. Lawrence, B., Torruellas, W . E., Cha, M., Sundheimer, M . L., Stegem an, G . I., Meth, J., Etem ad, S., & Baker, G . (1994) Phys. Rev. Lett. 73, 597{600.
44. Liess, M., Jeglinski, S., Vardeny, Z. V., Ozaki, M., Yoshino, K., Ding, Y., & Barton, T . (1997) Phys. Rev. B 56, 15712{15724.
45. Shukla, A., Ghosh, H., & Mazum dar, S. (2003) Phys. Rev. B 67, 245203.
46. Ohno, K . (1964) Theor. Chim . Acta 2, 219{227.
47. Monkm an, A . P., Burrows, H . D., Hartwell, L . J., Horsburgh, L . E., Hamblett, I., & Navaratnam, S. (2001) Phys. Rev. Lett. 86, 1358{1361.